

# Physics-inspired Estimation of Optimal Cloth Mesh Resolution

DIYANG ZHANG, Style3D Research, China

ZHENDONG WANG\*, Style3D Research, China

ZEGAO LIU, Style3D Research, China

XINMING PEI, State Key Laboratory of CAD & CG, Zhejiang University, China and Style3D Research, China

WEIWEI XU, State Key Laboratory of CAD & CG, Zhejiang University, China

HUAMIN WANG, Style3D Research, China



(a) Golden Grace

(b) Blue Ballet

(c) Mint Melody

(d) Pinkish Puff

Fig. 1. By leveraging experimental wrinkle theories, our method computes nonuniform mesh resolutions tailored to fabric properties and ensures smooth transitions across local resolutions introduced by garment-making techniques. Applied to complex garments like shirring dresses and down coats, our approach delivers visually accurate results while significantly reducing computational costs.

In this paper, we tackle an important yet often overlooked question: What is the optimal mesh resolution for cloth simulation, without relying on preliminary simulations? The optimal resolution should be sufficient to capture fine details of all potential wrinkles, while avoiding an unnecessarily high resolution that wastes computational time and memory on excessive vertices. This challenge stems from the complex nature of wrinkle distribution, which varies spatially, temporally, and anisotropically across different orientations. To address this, we propose a method to estimate the optimal cloth mesh resolution, based on two key factors: material stiffness and boundary conditions.

To determine the influence of material stiffness on wrinkle wavelength and amplitude, we apply the experimental theory presented by Cerdá and Mahadevan [2003] to calculate the optimal mesh resolution for cloth fabrics. Similarly, for boundary conditions influencing local wrinkle formation, we

use the same scaling law to determine the source resolution for stationary boundary conditions introduced by garment-making techniques such as shirring, folding, stitching, and down-filling, as well as predicted areas accounting for dynamic wrinkles introduced by collision compression caused by human motions. To ensure a smooth transition between different source resolutions, we apply another experimental theory from [Vandeputte et al. 2011] to compute the transition distance. A mesh sizing map is introduced to facilitate smooth transitions, ensuring precision in critical areas while maintaining efficiency in less important regions. Based on these sizing maps, triangular meshes with optimal resolution distribution are generated using Poisson sampling and Delaunay triangulation. The resulting method can not only enhance the realism and precision of cloth simulations but also support diverse application scenarios, making it a versatile solution for complex garment design.

CCS Concepts: • Computing methodologies → Physical Simulation; Modeling Methodologies.

Additional Key Words and Phrases: mesh resolution, wrinkle wavelength, material stiffness

## ACM Reference Format:

Diyang Zhang, Zhendong Wang, Zegao Liu, Xinming Pei, Weiwei Xu, and Huamin Wang. 2025. Physics-inspired Estimation of Optimal Cloth Mesh Resolution. In *Special Interest Group on Computer Graphics and Interactive Techniques Conference Conference Papers (SIGGRAPH Conference Papers '25)*, August 10–14, 2025, Vancouver, BC, Canada. ACM, New York, NY, USA, 11 pages. <https://doi.org/10.1145/3721238.3730619>

## 1 Introduction

Recent advancements in physics-based cloth simulation [Wang 2021; Wu et al. 2022] have significantly improved efficiency and quality,

Permission to make digital or hard copies of all or part of this work for personal or classroom use is granted without fee provided that copies are not made or distributed for profit or commercial advantage and that copies bear this notice and the full citation on the first page. Copyrights for components of this work owned by others than the author(s) must be honored. Abstracting with credit is permitted. To copy otherwise, or republish, to post on servers or to redistribute to lists, requires prior specific permission and/or a fee. Request permissions from [permissions@acm.org](mailto:permissions@acm.org).

SIGGRAPH Conference Papers '25, Vancouver, BC, Canada

© 2025 Copyright held by the owner/author(s). Publication rights licensed to ACM.  
ACM ISBN 979-8-4007-1540-2/2025/08  
<https://doi.org/10.1145/3721238.3730619>

enabling higher resolutions and supporting more vertices. However, a crucial question remains underexplored: *what is the optimal resolution for simulating a cloth mesh?*

Low-resolution meshes fail to capture fine wrinkle details, leading to visual artifacts like locking, while excessive resolution results in unnecessary computational overhead and memory usage. Ideally, high-resolution meshes should be applied selectively in regions with intricate wrinkle details. As demonstrated in [Wang 2021], simulating a stirred dress similar to the one in Fig. 1, requires a full resolution of less than 1 mm, which can take several seconds per frame to compute, even with GPU acceleration. Since wrinkle characteristics vary in size and orientation, the mesh resolution should adapt to these variations, potentially in a non-uniform and anisotropic manner, as shown in Fig. 6. A simple method for determining optimal resolution involves running a full-resolution simulation followed by mesh simplification. While this reduces memory usage, it does not address computational inefficiency. A more practical approach is to begin with a low-resolution simulation and adaptively refine or coarsen the mesh [Narain et al. 2012] as wrinkles form. This reduces computational costs while preserving detail but faces a critical limitation: refinement criteria depend on wrinkles simulated at low resolution, which may lack accuracy due to insufficient initial detail. For example, Fig. 20(c) illustrates excessive wrinkles persisting on the lap, while the bottom of the dress remains too coarse to form sufficient wrinkles for refinement. Furthermore, dynamic remeshing involves localized, sequential mesh operations that are difficult to parallelize, limiting performance on GPUs.

In this paper, we aim to address a key question: can we estimate the optimal mesh resolution for a cloth simulation in the worst-case scenario once and for all, without performing any preliminary simulations? Since the optimal resolution is directly tied to wrinkle size, i.e., the wrinkle wavelength, this question can be reframed: *what is the smallest possible wrinkle wavelength that could emerge on a cloth mesh during simulation?* As established in [Cerda and Mahadevan 2003; Vandeparre et al. 2011], wrinkle wavelength is influenced by two primary factors: *material stiffness* and *boundary conditions*. Material stiffness plays a clear role in determining wrinkle wavelength—lower bending stiffness results in finer, smaller wrinkles. Boundary conditions, on the other hand, introduce additional complexity to wrinkle formation. In real-world garments, boundary conditions often arise from garment-making techniques such as gathering, Shirring, and creasing, which are intentionally applied to create stationary wrinkles. The wavelengths of these wrinkles can typically be estimated based on the nature of these techniques. In addition, dynamic boundary conditions also play a significant role in simulations, particularly those driven by human motion. For instance, as an arm bends, fine wrinkles tend to form in the inner elbow of a sleeve, as illustrated in Fig. 13.

To address challenges, we present a novel framework for estimating the optimal cloth resolution before simulation, accounting for factors such as material stiffness, stationary boundary conditions from garment-making techniques, and dynamic collisions. For each cloth piece in a garment, we compute the characteristic wavelength [Cerda and Mahadevan 2003] based on its material stiffness to estimate the corresponding optimal global resolution. Our method also supports anisotropic materials by estimating the

optimal resolution for each anisotropic direction. For stationary boundary conditions resulting from garment-making techniques, such as Shirring, folding, stitching and down-filling, we define specific rules for each technique to determine the local resolution along the boundaries. Using wrinkle transition theories [Vandeparre et al. 2011], we calculate the associated propagation distance to ensure accurate simulation. Different resolutions on a cloth piece transition smoothly, resulting in a continuous sizing map that encodes both global and local resolution information. Using this sizing map, we generate a triangular cloth mesh through a two-step process: Poisson sampling and Delaunay triangulation. As shown in Fig. 1, the resulting nonuniform resolution cloth meshes effectively handle complex garments, capturing intricate wrinkle patterns produced by various garment-making techniques. We demonstrate the effectiveness of our method by comparing it to high-resolution simulations and dynamic remeshing techniques.

## 2 Related Work

Efficient and high-quality cloth simulation has been a longstanding focus. Achieving high-quality simulations requires two key factors: sufficient mesh resolution and accurate numerical solutions. Conversely, achieving efficiency depends on minimizing mesh resolution and employing fast numerical methods. To address the trade-off between simulation performance and realism, various approaches have been developed, including advanced linear and nonlinear numerical algorithms, fine wrinkle enhancements for coarse simulations, sophisticated finite element methods, and dynamic remeshing techniques.

Many methods have been proposed to improve the efficiency of physics-based cloth simulation, from early works on implicit integration for linearized simulations [Baraff and Witkin 1998; Choi and Ko 2002] to modern approaches [Bouaziz et al. 2014; Macklin et al. 2016] and descent methods for nonlinear simulations [Lan et al. 2023; Wang and Yang 2016]. Multilevel and multigrid solvers [Chen et al. 2021b; Tamstorf et al. 2015; Wang et al. 2018; Wu et al. 2022] have also been specially designed for improving accuracy of high-resolution simulations. Various methods have also been developed to enhance coarse simulations with fine-grained wrinkles. Post-processing methods estimate realistic wrinkles using various additional inputs, such as triangle stretch tensors [Rohmer et al. 2010], user-defined wrinkle patterns [Hadap et al. 1999], wrinkle path tracking [Bergou et al. 2007; Rémillard and Kry 2013], and amplitude-phase fields [Chen et al. 2021a, 2023]. Some methods [Müller and Chentanez 2010; Wang 2021; Zhang et al. 2022] simulate quasistatic fine wrinkles on high-resolution patches constrained to coarse simulations, while others [Gillette et al. 2015] compute temporally adaptive reference shapes to generate dynamic wrinkles. Data-driven methods [Popa et al. 2009; Wang et al. 2010; Zurdo et al. 2013] and learning-based models [Lahner et al. 2018; Oh et al. 2018] predict high-frequency details like fine folds and wrinkles from the space-time deformation of coarse garments but often lack direct physical fidelity. Recently, graph neural networks (GNNs) have emerged as scalable solutions for adaptive mesh discretization in dynamic simulations [Pfaff et al. 2020] and addressing physical discrepancies between simulations of different resolutions [Yu and

Wang 2024]. Dynamic remeshing is a common approach for adaptive refinement during simulations [Narain et al. 2013, 2012; Pfaff et al. 2014; Wicke et al. 2010], efficiently allocating computational resources. Sizing fields, represented as metric tensor fields, guide adaptive mesh resolution to meet finite element accuracy requirements [Labelle and Shewchuk 2003; Shewchuk 2002b; Wicke et al. 2010]. Recent advancements in finite element methods [Le et al. 2023] have improved cloth simulation accuracy and efficiency without frequent remeshing. Additional innovations include surface simplification with intrinsic error metrics [Liu et al. 2023], triangle mesh developability [Stein et al. 2018], and intrinsic triangulation navigation [Sharp et al. 2019].

The physics of wrinkling in thin shells has been extensively studied. Cerdá and Mahadevan [Cerdá and Mahadevan 2003] introduced a scaling law relating wrinkle wavelength to material properties, forming the basis for subsequent studies [Healey et al. 2013; Li and Healey 2016; Wang et al. 2019] and extensions to complex geometries like rotationally symmetric 3D shapes [Aharoni et al. 2017; Paulsen et al. 2016]. However, these models assume constant wrinkle direction and wavelength, limiting their applicability to complex fabrics like draped garments. Zuenko and Harders [2019] extended these methods to materials with soft substrates, predicting wrinkle frequency using film-to-substrate shear modulus ratios [Vandeparre et al. 2011], but these approaches struggle with scenarios lacking a substrate or involving complex contact-driven wrinkles. Studies on buckling phenomena in thin-sheet mechanics [Choi and Ko 2002; Vetter et al. 2014] provide insights into fabric deformation under compressive strain and fine wrinkle generation. By integrating experimental theories of wrinkle wavelength and transition distances, our method optimizes cloth mesh resolution while maintaining computational efficiency.

### 3 Experimental Wrinkle Theories

Experimental physics offers practical theories on wrinkle formation, but physics-based simulations primarily focus on optimizing high-resolution simulations or enhancing coarse ones with added details. Few studies address optimal resolution setting. This section outlines the experimental wrinkle theories underpinning our method.

#### 3.1 Characteristic Wrinkle Wavelength

Cerdá and Mahadevan [2003] revealed that the characteristic wavelength  $\lambda$  and amplitude  $A$  of wrinkles in a deformed thin sheet is determined by the balance between the bending stiffness  $B$ , the elastic stiffness  $K$  of the supporting elastic substrate and an imposed transversal compressive strain  $\delta = \Delta/W$ ,

$$\lambda \sim (B/K)^{1/4}, \quad A \sim \lambda \sqrt{\delta}. \quad (1)$$

Bending penalizes short wavelengths, while the substrate suppresses long ones, resulting in intermediate wrinkle scales. The scaling law derivation are actually based on sheet experiments without a substrate. As shown in Fig. 2 (a), a slender elastic sheet, such as a polyethylene strip, with thickness  $t$ , width  $W$ , and length  $L$  ( $t \ll W \ll L$ ), remains flat under longitudinal strain  $\gamma < \gamma_c$ , the critical strain. Beyond this point ( $\gamma > \gamma_c$ ), wrinkles form due to strain incompatibility from the Poisson effect. Assuming that the out-of-plane displacement of the initially flat sheet is  $\zeta(x, y)$ , where

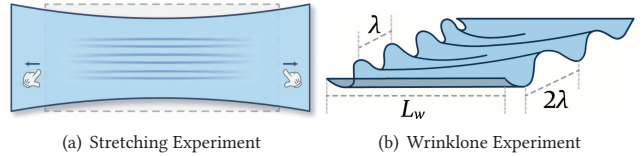


Fig. 2. Experiments. (a) A thin sheet with length  $L$  and width  $W$  is stretched, resulting in a displacement  $\Delta$  in the width direction. (b) A thin sheet forms wrinkles with a wavelength of  $\lambda$  on the left and  $2\lambda$  on the right, with a transition distance of  $L_w$  between them.

$x \in (0, L)$  is the coordinate along the sheet measured from one end and  $y \in (0, W)$  is the coordinate perpendicular to it measured from its central axis, the functional to be extremized is  $\mathcal{U} = U_B + U_S - \mathcal{L}$ , where  $U_B = \frac{1}{2} \int_A B (\partial_y^2 \zeta)^2 dA$  and  $U_S = \frac{1}{2} \int_A T(x) (\partial_x \zeta)^2 dA$  are respectively the bending energy and the stretching energy under tension  $T(x)$ . Wrinkling in the  $y$ -direction satisfies the inextensibility condition which is incorporated via the Lagrangian  $\mathcal{L}$ . Based on the observation that wrinkling pattern  $\zeta$  is periodic away from the free edges, the solutions by minimizing  $\mathcal{U}$  are  $\lambda = 2\sqrt{\pi} \left( \frac{B}{T/L^2} \right)^{1/4}$  and  $A = \frac{\sqrt{2}}{\pi} \lambda \sqrt{\delta}$ . Please refer to [Cerdá and Mahadevan 2003] for detailed derivations. The expression for the stretching energy of a thin sheet is analogous to the form of the energy in an elastic foundation supporting a thin sheet,  $U_F \sim \frac{1}{2} \int_A K \zeta^2 dA$ . Comparing  $U_S$  and  $U_F$ ,  $K \sim T/L^2$  is the stiffness of the effective elastic foundation for the stretched sheet. Cerdá and Mahadevan [2003] introduced a dimensionless function  $f(\lambda/l_p)$  with a penetration length  $l_p$  to characterize the system geometry of various substrates, leading to

$$K = E_s f(\lambda/l_p)/l_p. \quad (2)$$

For an incompressible substrate,  $f(\lambda/l_p) \sim \lambda^2/l_p^2$ .

#### 3.2 Wavelength Propagation

Thin sheets under boundary confinement exhibit a universal, self-similar hierarchy of wrinkles, governed by "wrinklons" [Vandeparre et al. 2011], localized zones where two wrinkles merge into one with a larger wavelength. Building on models of period-doubling transitions, wrinklons can act as fundamental building blocks, with the global wrinkling pattern emerging from their self-assembly. Each wrinklon is characterized by a size  $L_w$ , the distance over which the wavelength increases from  $\lambda$  to  $2\lambda$ , as shown in Fig. 2 (b). Experiments with thin plastic sheets constrained by sinusoidal clamps, imposing wavelengths  $\lambda$  (amplitude  $A$ ) and  $2\lambda$  (amplitude  $2A$ , respectively), reveal that the normalized wrinklon size  $L_w/\lambda$  scales as  $\sqrt{A/h}$ . Since  $A \sim \lambda \sqrt{\delta}$ , this scaling implies  $L_w \propto \lambda^{3/2}$ . Actually, the patterns with increasing wrinkle size with respect to distance  $x$  follow a power law  $\lambda \sim x^m$ , which emerges from a balance between bending and stretching energies and connects the properties of individual wrinklons to the global features of the wrinkling cascade. In the experiment of a hanging curtain, the size of a single wrinklon, with a characteristic area  $L_w \lambda$ , is derived by minimizing the total energy  $U_{tot} = (u_s + u_b)L_w \lambda$  with respect to  $L_w$ . The computation of stretching energy varies between light and heavy

curtains. For a light curtain, the relationship  $\lambda(x) \sim x^{2/3}(h^2/\delta)^{1/6}$  results in a power-law scaling  $\lambda \propto x^{2/3}$ . Conversely, for a heavy curtain,  $\lambda(x) \sim x^{1/2}(B/T)^{1/4}$  yields the scaling  $\lambda \propto x^{1/2}$ . Detailed derivations can be found in [Vandeparre et al. 2011].

## 4 Our Method

Fabrics with varying stiffness require different mesh resolutions: stiff materials form coarse, large wrinkles, while soft ones produce fine details. Uniform resolution is inefficient—either wasting computation or missing accuracy. Our method, grounded in experimental wrinkle theories, adjusts mesh resolution based on material stiffness and garment features like design details or high-collision zones (e.g., elbows), without the need for preliminary simulations or dynamic remeshing.

### 4.1 Estimating Optimal Cloth Resolution

To accurately capture wrinkles, cloth mesh resolution must match wrinkle wavelengths, with edge lengths smaller than or comparable to the smallest wavelength. Although wrinkles form dynamically, their characteristic wavelength can be predicted using the scaling law in Eq. 1, guiding our method to estimate optimal cloth resolution.

**4.1.1 Optimal Resolution.** The optimal cloth resolution is defined as the critical resolution where further increases yield minimal accuracy gains. As shown in Fig. 18, coarse resolutions result in noticeable inaccuracies, but as the resolution approaches the critical level, the results closely align with the ground truth. Beyond this point, additional refinement offers diminishing improvements.

Given the characteristic wrinkle wavelength  $\lambda$  and amplitude  $A$ , we calculate the optimal mesh resolution as  $r_{opt} = \sqrt{\lambda^2/16 + A^2}$ , derived using the Pythagorean theorem, as illustrated in Fig. 4. Since  $A$  is proportional to  $\lambda$ , which depends on the cloth mesh’s shape, we approximate  $r_{opt} \sim c\lambda$ , where  $c$  incorporates the compression ratio and mesh geometry. To estimate the optimal cloth mesh resolution, we propose a forward method based on fabric material stiffness using the scaling law in Eq. 1. At first glance, applying the wrinkle wavelength scaling law for thin sheets on elastic substrates to fabrics might seem questionable in principle, given that fabrics typically lack an explicit substrate. The key distinction in the wrinkle scaling laws with versus without a substrate lies in the presence of a dimensionless geometric function  $f(\lambda/l_p)$ , which is used to compute the elastic stiffness  $K$ . However, due to the near-incompressibility of most fabrics, we observe, consistent with the thin sheet stretching test in [Cerda and Mahadevan 2003], that the compressive resistance in the direction orthogonal to stretching acts analogously to a substrate. This resistance penalizes long wavelengths, much like an elastic substrate in the compressed skin model in [Cerda and Mahadevan 2003]. As a result, it can be modeled as an virtual elastic substrate with thickness

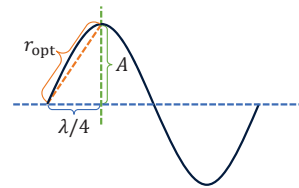


Fig. 4. Optimal resolution calculated using characteristic wrinkle wavelength and amplitude based on the Pythagorean theory.

$h_s$  and Young’s modulus  $E_s$ , inferred from the fabric’s Young’s modulus  $E$ . Consequently, in our method, we adopt the dimensionless function  $f(\lambda/l_p) \sim \lambda^2/l_p^2$  typically used for incompressible material, to characterize the geometry of fabrics. Based on this model, we recommend using a minimum mesh resolution of 2.5mm in our cloth simulation system. Furthermore, we generalize  $f(\lambda/l_p)$  as

$$f(\lambda/l_p) = d_1(\lambda/l_p)^2 + d_2, \quad (3)$$

where  $d_1$  and  $d_2$  are two dimensionless parameters. Substituting Eq. 3 into Eq. 2 and incorporating the scaling law in Eq. 1, i.e.  $\lambda \sim (B/K)^{1/4}$ , we arrive at the expression  $(d_1 l_p^{-3})\lambda^6 + (d_2 l_p^{-1})\lambda^4 = B/E_s$ . Recalling that the optimal resolution is proportional to the characteristic wrinkle wavelength, i.e.  $r = c\lambda$ , and assuming the substrate’s Young’s modulus is proportional to the fabric’s Young’s modulus, i.e.  $E_s = gE$ , the scaling factors  $c$  and  $g$ , along with the substrate penetration length  $l_p$  and thickness  $h_s$ , can be absorbed into two effective parameters  $c_1$  and  $c_2$ . This leads to the simplified relation:

$$c_1 r^6 + c_2 r^4 = y. \quad (4)$$



Fig. 3. Five fabrics with varying material stiffnesses are tested, ranging from stiffest (top) to softest (bottom). The middle column shows simulation results using resolutions calculated by our method, which closely match the high-quality results in the right column, simulated with a minimal resolution of 2.5 mm. In contrast, the left column, using resolutions twice as ours, exhibits low-quality wrinkles with noticeable locking artifacts.

where  $y = B/E$  represents the fabric's bending-to-stretching stiffness ratio. Thus, given a fabric with Young's modulus  $E$  and bending stiffness  $B$ , the optimal resolution for cloth simulation is determined by  $c_1$  and  $c_2$ , which reflect the geometric properties of the system.

For fabrics following the Kirchhoff-Love thin shell theory, where  $y = \frac{h^3}{12(1-\nu^2)}$ , and assuming  $r$  scales monotonically with  $y$ , thicker, stiffer fabrics require coarser resolutions, while thinner, softer fabrics require finer resolutions. This aligns with typical fabric behavior in simulations. From Eq. 4, fabrics with the highest  $B$  and smallest  $E$  require the coarsest resolution, while those with the lowest  $B$  and largest  $E$  require the finest resolution. These extremes are defined by system designers, and in our system they are:  $E \in [2e^3, 2e^6] \text{ N/m}^2$ ,  $B \in [1e^{-9}, 1e^{-3}] \text{ N} \cdot \text{m}$ ,  $r \in [2.5, 50] \text{ mm}$ . Using these values,  $c_1$  and  $c_2$  can be determined by solving the following equation,

$$\begin{bmatrix} c_1 \\ c_2 \end{bmatrix} = \det^{-1} \begin{bmatrix} r_{min}^4 & -r_{max}^4 \\ -r_{min}^6 & r_{max}^6 \end{bmatrix} \begin{bmatrix} y_{max} \\ y_{min} \end{bmatrix}$$

where  $\det = r_{max}^4 r_{min}^4 (r_{max} + r_{min})(r_{max} - r_{min})$ . In our method, their values are  $c_1 = 32.08 \text{ m}^{-3}$  and  $c_2 = -1.876e^{-4} \text{ m}^{-1}$ . The relationship between the optimal resolution and material stiffness is depicted in Fig. 5. For a fabric with known Young's modulus  $E$  and bending stiffness  $B$ , the optimal resolution can be computed as  $r_{opt} = r(y, c_1, c_2)$  using Eq. 4. Fig. 3 demonstrates that our method effectively reproduces high-resolution results across fabrics with varying material stiffnesses.

**4.1.2 Anisotropy.** For isotropic fabrics, the estimated optimal resolution produces uniform triangular meshes. However, orthotropic fabrics require distinct weft and warp resolutions. Applying the smaller resolution uniformly results in overly dense meshes. Our method addresses this by tailoring mesh resolutions to each direction's anisotropic properties. As shown in Fig. 6, for anisotropic fabric, tailoring fine weft and coarse warp resolutions achieves results comparable to uniform fine resolution, significantly outperforming uniform coarse resolution.

**4.1.3 Locking Issue.** In coarse fabric simulations, the locking issue arises from strong in-plane compressive resistance, restricting bending and causing artifacts. Reducing compressive resistance within a reasonable strain range alleviates this issue, as implemented in our method. However, coarse simulations still fail to match the accuracy of fine simulations (Fig. 3(a)), and without adjustment, locking worsens as illustrated in Fig. 7. While addressing locking is not the primary focus, our approach inherently mitigates it by enabling resolutions that balance performance and accuracy, demonstrating its robustness.

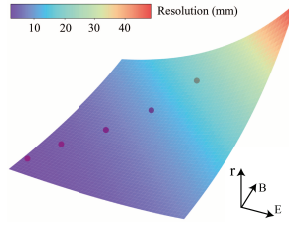


Fig. 5. Cloth resolution  $r$  as a function of  $B$  and  $E$ .



Fig. 6. For an anisotropic fabric, we calculate a fine resolution for the weft direction and a coarse resolution for the warp direction. This nonuniform resolution achieves a result comparable to that of a uniform fine resolution while significantly outperforming a uniform coarse resolution.



Fig. 7. The fabric, identical to that in the fifth row in Fig. 3, has low bending stiffness and high stretching stiffness. Despite exacerbated locking issue due to the absence of locking adjustments, simulations with the optimal resolution closely match those using the finest resolution.

## 4.2 Boundary Conditions

Garment-making techniques like Shirring, folding, stitching, and down-filling introduce localized stresses and constraints, altering fabric deformation and creating distinct wrinkle patterns. These effects extend beyond local areas, influencing overall fabric behavior and appearance. Uniform mesh resolutions often lead to high computational costs or insufficient detail. Adapting resolutions to these features with smooth transitions achieves: *enhanced precision*, capturing intricate wrinkles; *improved realism*, preserving visual and physical authenticity of the fabric under varying stresses; and *greater efficiency*, focusing higher resolution where needed while reducing computational overhead without compromising accuracy.

**4.2.1 Resolution Transition.** The scaling law for wrinkle wavelength transition distance  $L_w$  from  $\lambda$  to  $2\lambda$  follows  $L_w(\lambda) \sim \lambda^2 \sqrt{T/B}$  for a fabric under tension  $T$ , and  $L_w(\lambda) \sim \lambda^{\frac{3}{2}} (\delta h^{-2})^{\frac{1}{4}}$  for a fabric with compressive ratio of  $\delta$ . In [Vandeparre et al. 2011], a power law  $\lambda \sim x^m$  describes wrinkle wavelength  $\lambda$  as a function of distance  $x$ . Since mesh resolution is proportional to wrinkle wavelength, we extend this relationship to mesh resolution changes from a source resolution, i.e.  $\Delta r = x^m$ . By setting  $r + L_w^m = 2r$ , the transition power  $m$  is derived as  $m = \frac{\log r}{\log L_w}$ , incorporating the scaling factor between  $r$  and  $\lambda$  into  $m$ . Essentially,  $m$  encapsulates the combined effects of the source resolution and the fabric's material stiffness.

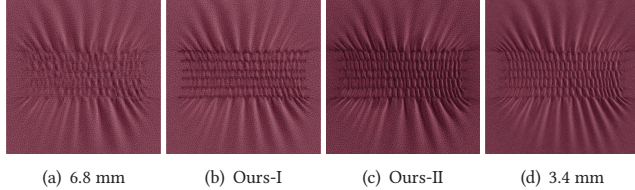


Fig. 8. (a) Uniform resolution of 6.72 mm. (b) Ours-I using our method to compute the source resolution on shirring lines. (c) Ours-II incorporates smooth transitions, resulting in seamless wrinkle patterns. (d) Uniform resolution of 3.36 mm. Our-II produces the smoothest shirring wrinkles among these approaches.

For a vertex at distance  $x$  from the source mesh resolution  $r$ , its resolution is computed as  $r + x^m$ . In general, given a fabric with base resolution  $r_f$ , if multiple source resolutions  $[r_0, \dots, r_n]$  originate from boundary conditions from garment-making techniques, the resolution at a vertex is calculated as  $r_v = \min(r_f, r_0 + x_0^{m_0}, \dots, r_n + x_n^{m_n})$ , where  $x_n$  is the distance from the vertex to the  $n$ th boundary condition, and  $m_n$  is its resolution transition power.

**4.2.2 Shirring.** Shirring, commonly used in garments like waistbands and cuffs (8), generates localized tension and compression, resulting in pronounced wrinkles and puckering. The wrinkle wavelength and amplitude depend on the combined effects of shirring stiffness and the base fabric stiffness, necessitating higher mesh resolution in these areas. To compute the source wavelength, the additional shirring stiffness  $E_{sh}$  and shrinkage ratio  $\rho_{sh}$  are incorporated. Using  $y_{sh} = \frac{B}{E+E_{sh}}$  in Eq. 4, the source resolution is calculated as  $r_{sh} = \rho_{sh}^n r(y_{sh}, c_1, c_2)$ , where  $n$  is a user-defined parameter, typically  $n = 1$  in our method.

**4.2.3 Folding.** Folding, often used for edge reinforcement in garment design, introduces sharp creases and layered structures (Fig. 9) that significantly affect local deformation. Along folding edges, where no compressive strain occurs, the resolution matches the base fabric. However, compression perpendicular to the edges generates fine wrinkles. To account for these, two parallel lines are added on either side of the folding edges, with minimal spacing (e.g., 0.5 mm), to capture the intricate folding details. At endpoints and high-curvature regions of curved folding edges, significant compression arises, producing distinct wrinkle patterns. To address this, the compressive strain is evaluated as  $\rho_{fd} = \Delta\theta/360$ , where  $\Delta\theta$  is the folding angle relative to a flat rest state. The source resolution is then calculated as  $r_{fd} = \rho_{fd} r_{ng}$ , where  $r_{ng}$  is the resolution of the point's neighborhood. Then, a directional transition is applied for these folding points. At endpoints, the transition follows the direction of the folding edge, while at high curvature points, it aligns with the normal of folding edges at those points. Only vertices in the forward direction are affected by the transition. This method ensures a smooth progression from folding resolution to the fabric's resolution, providing accurate and seamless representation of deformation.

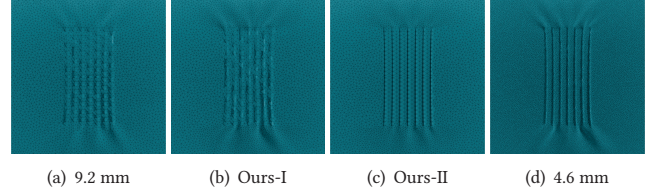


Fig. 9. (a) Uniform resolution of 9.2 mm. (b) Ours-I applies resolution transition at endpoints. (c) Ours-II incorporates parallel lines alongside bending edges. (d) Uniform resolution of 4.6 mm. Ours-II produces the smoothest folding wrinkles among these approaches.

**4.2.4 Stitching.** Stitching lines locally reinforce fabric but can also induce wrinkles due to compressive forces along seams, necessitating mesh refinement. The affected area extends a specific width on both sides of the seam. Stitching lines with a compressive ratio can be modeled as shirring edges. When a longer line is sewn to a shorter one, the compressive strain  $\rho_s = l_s/l_l$  (where  $l_s$  and  $l_l$  are the length of the short and the long lines) determines the source resolution of the longer line. Resolution propagation is applied exclusively to the fabric side with the longer line, ensuring accurate and efficient wrinkle representation.

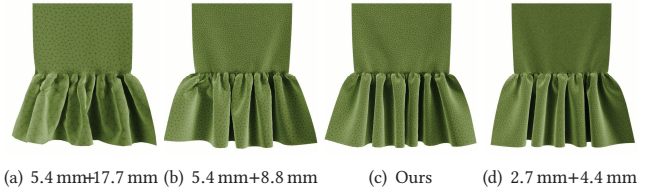
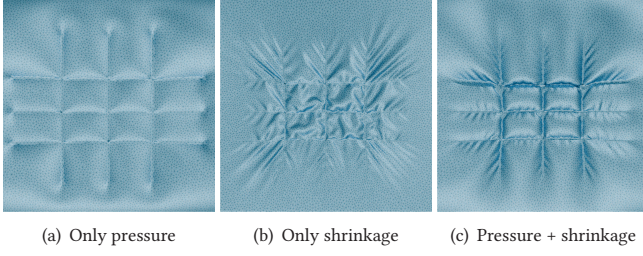


Fig. 10. In this case, the long-short stitching introduces a compressive ratio. (c) Our method applies resolution transition to (b), producing a result comparable to the finest simulation (d) and outperforms both (a) and (b).

**4.2.5 Down-filling.** In a down coat, multiple stitched packs are filled with down. Along the stitching lines, a compressive ratio is applied to keep the packs tight. Our method for the shirring technique is used to calculate the source resolution and transition distance along these stitching lines. Additionally, the internal pressure from down filling stretches the fabric, reducing wrinkle formation and diminishing wrinkle transitions. To account for this, we incorporate the down-filling pressure  $p$  into the calculation of the transition power  $m' = 2^p m$ . In our method, increasing pressure is equivalent to increasing the fabric's thickness, which effectively raises the bending stiffness. This reduces the transition distance  $L'_w = (L_w)^{2^{-p}}$ , thereby accelerating the resolution transition along the stitching lines. As shown in Fig. 11, higher pressure causes wrinkles from the stitching lines to dissipate more quickly.

**4.2.6 High-collision Areas.** The core of our method is to estimate an optimal mesh resolution before running a simulation, which inherently cannot account for wrinkles caused by dynamic contacts or collisions that cannot be predicted beforehand. Even though, we



(a) Only pressure (b) Only shrinkage (c) Pressure + shrinkage

Fig. 11. Incorporating pressure and small compressive ratios for down fabrics, our method improves resolution transitions for down-filled areas, ensuring more accurate simulations.

observe that most collision-induced wrinkles, including those from body-clothing contact and multilayer interactions, are well handled by our approach. As demonstrated in Fig. 12, in the challenging scenario where two layers of cloth are twisted by a rotating sphere and form gathered wrinkles, our method remains beneficial. However, for garments on human bodies, areas with extreme collisions, such as the elbow region, can often be anticipated. As shown in Fig. 13, we manually label an elbow area and use our method to assign a specialized mesh resolution by estimating compression strain from collisions. Currently, our method does not automatically identify high-collision areas or their characteristic compression. This limitation highlights an opportunity for future work: training a neural network to automatically detect high-collision regions and their associated compressive strains using human motions and pattern libraries with semantic labels.



(a) Fine: 5.0 mm (b) Ours: 7.83 mm (c) Coarse: 15.6 mm

Fig. 12. Two cloth layers—orange (inner) and blue (outer)—are twisted by a rotating sphere, forming gathered wrinkles. This challenging scenario highlights the strength of our method. Compared to the fine-resolution simulation (a), our approach (b) effectively captures collision-induced wrinkles from multilayer interactions, whereas the coarse simulation (c) results in noticeable artifacts.

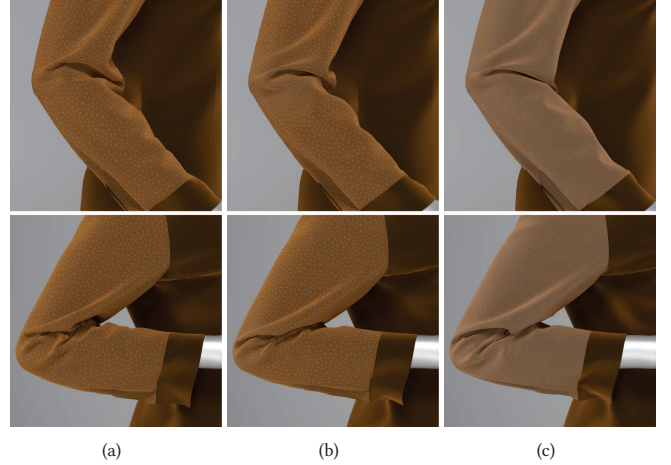


Fig. 13. We manually label the elbow area and apply our method to assign a specialized mesh resolution based on predicted compression strain from collisions. (b) Our results produce smooth wrinkles comparable to the uniform fine resolution simulation (c) and significantly outperform the uniform coarse resolution simulation (a).

### 4.3 Sizing Maps

Given the fabric’s material stiffness and boundary conditions from garment-making techniques, our method computes the fabric’s optimal resolution, boundary resolutions, and transition power parameters. This information is transformed into a sizing map using the transition rule described in Section 4.2.1, as shown in Fig. 14(b). The sizing map provides a continuous representation of resolution distribution across the cloth mesh. To generate the triangular mesh, we first sample the sizing map using the fast Poisson disk sampling algorithm [Bridson 2007], ensuring that the average vertex spacing locally aligns with the sizing values. The resulting point cloud, along with boundary constraints, is then input into triangulation tools such as the Triangle library [Shewchuk 2002a] to produce a triangular cloth mesh adhering to Delaunay triangulation rules.

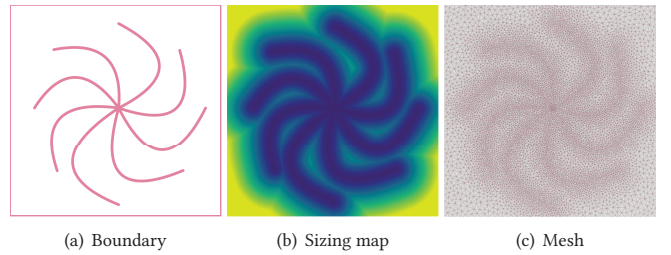


Fig. 14. (a) Given a fabric piece with square boundary and inner curved stirring lines, we calculate the fabric resolution and stirring resolution, ensuring a smooth transition between the two to generate a (b) sizing map. Using this sizing map, we perform Poisson sampling to distribute vertices, followed by Delaunay triangulation to create (c) the mesh. The resulting mesh is then used for simulation, producing the result shown in Fig. 15 (c).

Table 1. The statistics of our examples include five complex garments and five fabrics. Using  $c_1 = 32.08 \text{ m}^{-3}$  and  $c_2 = -1.876e^{-4} \text{ m}^{-1}$ , we calculate the optimal resolution based on the fabric’s bending stiffness ( $B : N \cdot m$ ) and Young’s modulus ( $E : N/m^2$ ). For garments, only the optimal resolution of the main fabric is listed. The full simulations use a fine resolution of 2.5 mm, except for the Wine Style dress example, which uses 5 mm. **NS** and **CH** represent average numerical solving (NS) and collision handling (CH) time per frame, respectively. Resolution unit: millimeter (mm). Time unit: millisecond (ms).

| Garments     | B           | E        | Ours |      |      | Full Sim |       |      | Fabrics | B          | E           | Ours     |      | Full Sim |       |
|--------------|-------------|----------|------|------|------|----------|-------|------|---------|------------|-------------|----------|------|----------|-------|
|              |             |          | Res. | # V  | NS   | CH       | # V   | NS   |         |            |             | Res.     | # V  | # V      |       |
| Wine Style   | $2.0e^{-6}$ | $3.0e^5$ | 7.83 | 59K  | 3.8  | 0.8      | 135K  | 8.6  | 1.7     | Dark Blue  | $1.6e^{-4}$ | $1.3e^5$ | 18.5 | 241      |       |
| Pinkish Puff | $2.0e^{-6}$ | $8.0e^5$ | 6.69 | 322K | 17.4 | 3.8      | 1.38M | 97.5 | 12.9    | Khaki      | $2.0e^{-5}$ | $5.0e^5$ | 10.5 | 708      |       |
| Mint Melody  | $7.8e^{-7}$ | $6.6e^4$ | 8.58 | 60K  | 4.8  | 1.2      | 400K  | 26.9 | 4.2     | Green      | $2.6e^{-6}$ | $2.0e^6$ | 6.00 | 2.1K     | 11.9K |
| Golden Grace | $2.0e^{-6}$ | $1.1e^5$ | 9.21 | 83K  | 5.1  | 1.3      | 586K  | 39.4 | 5.4     | Light Blue | $3.2e^{-7}$ | $8.2e^6$ | 3.61 | 5.8K     |       |
| Blue Ballet  | $2.5e^{-6}$ | $1.1e^5$ | 9.55 | 82k  | 4.9  | 1.6      | 876K  | 60.8 | 7.4     | Rose       | $4.0e^{-8}$ | $1.6e^7$ | 2.70 | 10K      |       |

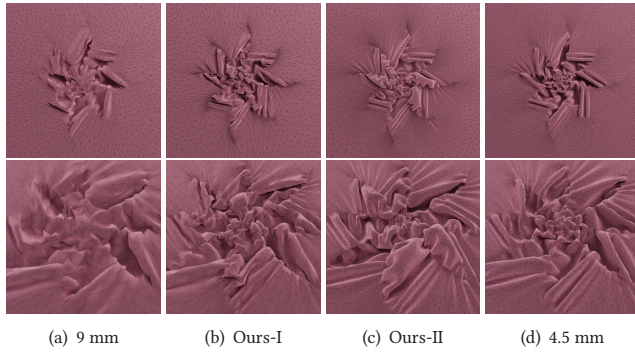


Fig. 15. We apply our method to compute the source resolution on shirring lines (b) and incorporate smooth transitions (c), resulting in seamless wrinkle patterns. This approach outperforms both the (a) uniform 9 mm resolution and the (d) uniform 4.5 mm resolution.

## 5 Results

In our cloth simulation system, we use Newton’s method with a 1/30s time step for implicit integration. Linear systems are solved using a preconditioned CG method with  $3 \times 3$  block diagonal preconditioning, terminating when the  $L_2$  residual norm falls below  $1e^{-5}$ . For anisotropic stretching, we adopt Baraff-Witkin’s linear elasticity model [Baraff and Witkin 1998], and for bending deformations, we use stable discrete bending models [Wang et al. 2023]. Complex collisions, such as those in shirring dresses and down coats in Fig. 1, are handled with an adaptive stepping strategy [Wu et al. 2020] for accuracy and efficiency. The system runs entirely on the GPU, except for remeshing operations performed on the CPU for comparison with dynamic remeshing methods. Experiments are conducted on a PC with an Intel Core i9-12900K CPU, 64GB RAM, and an NVIDIA GeForce GTX 3090 GPU.

### 5.1 Performance Evaluation

Our method generates garment meshes with adaptive optimal resolutions, balancing simulation realism and efficiency. Compared to uniform fine-resolution simulations at 2.5 mm, our approach significantly reduces vertex counts while maintaining comparable accuracy. Table 1 summarizes five garment and fabric examples,

demonstrating bending stiffness  $B$ , Young’s modulus  $E$ , optimal resolutions, and vertex counts. We separate total computation time into numerical solving and collision handling, demonstrating reduced numerical complexity and improved collision detection without compromising accuracy. Compared to uniform fine resolution, our estimated optimal resolutions achieve a  $2 - 10x$  speedup in numerical solving and  $2 - 4x$  in collision handling. Additionally, in the Wine Style example, each remeshing process takes 1–2 seconds on average, confirming that dynamic remeshing significantly slows down the simulation.

### 5.2 Validation

We validate our method through key experiments, including the stretching thin sheet [Cerda and Mahadevan 2003], the hanging curtain [Vandeparre et al. 2011].

*Stretching Test.* We conduct a stretching test on a rectangular cloth piece, stretched by 12.78% along its long edge, using the St.VK hyperelastic model, as also employed in [Chen et al. 2021a]. Based on the scaling law [Cerda and Mahadevan 2003], our calculated mesh resolution of 3.8 mm produces 6 wrinkles, closely matching the 7 wrinkles from a finer 2.5 mm mesh. In contrast, a coarser 5 mm mesh generates only 4 wrinkles, lacking accuracy, as shown in Fig. 16.

*Hanging Curtain.* In our method, each wrinkle wavelength corresponds to a specific mesh resolution, with smooth transitions matching the wrinkle wavelength transition distance [Vandeparre et al. 2011]. As shown in Fig. 17, a compressed hanging curtain generates varying wrinkle wavelengths from top to bottom. Our method smoothly transitions from the highest resolution at the compressed top edge to coarser resolutions, enabling high-quality wrinkle simulations. In contrast, uniform mesh resolution produces lower-quality wrinkles. To further validate our method, we conduct a quantitative experiment to assess the transition distance. As illustrated in Fig. 18(d), our computed transition distances remain in close agreement with the measured values across varying bending stiffness.

### 5.3 Comparisons

To evaluate the effectiveness of our method, we compare our method to direct high-resolution simulation and dynamic remeshing during simulation runtime.

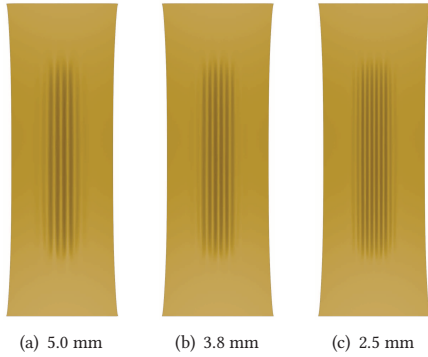


Fig. 16. A rectangular cloth piece is stretched by 12.78% along its long edge, using the St.VK hyperelastic model, as employed in [Chen et al. 2021a]. Our calculated mesh resolution of 3.8 mm produces 6 wrinkles, closely matching the 7 wrinkles from a finer 2.5 mm mesh. In contrast, a coarser 5 mm mesh generates only 4 wrinkles, lacking accuracy.



Fig. 17. A compressed hanging curtain generates varying wrinkle wavelengths from top to bottom. Our method smoothly transitions from the highest resolution at the compressed top edge to coarser resolutions, enabling high-quality wrinkle simulations. In contrast, uniform mesh resolution produces lower-quality wrinkles.

**5.3.1 High-Resolution Simulation.** As shown in Fig. 19, we apply our method to simulate three intricate garments: a shirring dress and a down coat. By using the estimated optimal nonuniform mesh resolution, our method produces high-quality wrinkle effects. In regions influenced by garment-making techniques, the mesh resolution is even higher than the minimal uniform resolution of 2.5 mm. In these areas, our method generates finer wrinkles than a uniform high-resolution simulation. Despite this, the total vertex count in our method is significantly lower, making it much more computationally efficient.

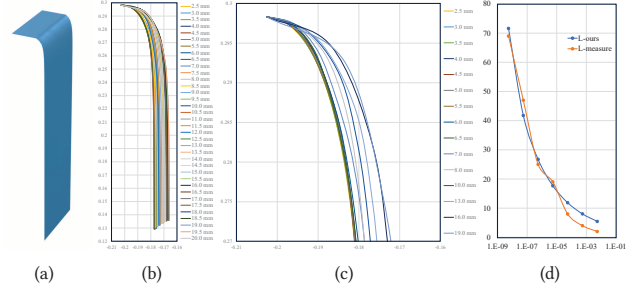


Fig. 18. (a) In a cantilever test, (b) mesh resolutions ranging from 20 mm to 2.5 mm are tested for a fabric with bending stiffness  $B = 2e^{-6} N \cdot m$  and Young's modulus  $E = 1e^6 N/m^2$ . (c) The results stabilized around 6.5 mm, with minimal accuracy gains beyond this point. In this case, our method estimated an optimal resolution of 6.45 mm, achieving an effective balance between accuracy and efficiency. (d) In the curtain test shown in Fig. 17, our computed transition distance is  $L_{ours} = 26.7\text{mm}$ , closely matching the measured value  $L_{mes} = 25\text{mm}$ . When varying the curtain's bending stiffness, the curve of our computed transition distance  $L - ours$  remains closely aligned with the measured values  $L - measure$ .

**5.3.2 Adaptive Mesh Refinement.** As shown in Fig. 20(c), dynamic remeshing [Narain et al. 2012] adjusts mesh resolution during simulation by refining high-compression and high-curvature regions while maintaining coarse resolution in flat areas. However, this approach introduces discontinuities, leading to oscillations and inconsistent cloth behavior. Coarse resolutions can make the cloth overly stiff, while fine resolutions can make certain areas excessively flexible, and frequent transitions between these states exacerbate instability. Moreover, each remeshing operation requires reconfiguring the simulation, including data structure updates and memory reallocation, resulting in significant computational overhead that often outweighs the benefits. Additionally, dynamic remeshing is not GPU-friendly, further limiting its efficiency. In contrast, our method delivers consistent, stable wrinkle effects without oscillations and achieves greater computational efficiency. Nevertheless, our method can provide initial meshes for dynamic remeshing techniques.

## 5.4 Conclusions

We present a physics-inspired method for optimal cloth mesh triangulation, balancing accuracy and efficiency. By leveraging experimental scaling laws, we compute nonuniform mesh resolutions based on fabric properties, garment-making techniques, and dynamic scenarios, ensuring smooth transitions via a sizing map. Our method reproduces realistic wrinkles while reducing computational costs compared to uniform high-resolution and dynamic remeshing approaches. Validations on complex garments, such as shirring dresses and down coats, showcase its ability to deliver visually accurate and efficient results without the discontinuities or overheads of traditional adaptive methods, offering a robust solution for cloth simulation in computer graphics and real-time applications. We conclude that the optimal mesh resolution estimated by our method effectively captures garment geometry. Our approach offers a novel

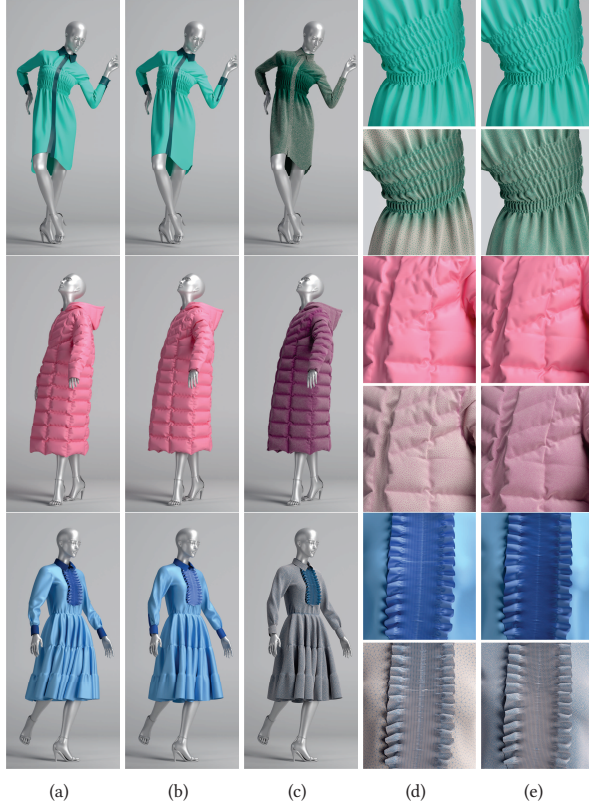


Fig. 19. We compare our method to full simulations with a uniform 2.5 mm resolution on garments with shirring and down filling. Full simulations, shown in (a) and zoomed-in (e), suffer from over-stretching due to convergence issues with overly dense meshes. Our method, shown in (b) with wireframe rendering and zoomed-in (d), achieves comparable results with significantly higher efficiency.

possibility to bridge real-world physics with geometric discretization in cloth simulation.

## 6 Limitations and Future Work

While our method offers an efficient and accurate solution for cloth simulation, it has some limitations. The precomputed mesh resolutions lack real-time adaptability to unexpected deformations, and the static transition regions may not fully capture abrupt fabric behavior changes. The method also struggles with dynamic environments involving unpredictable interactions, such as flowing fabrics, and does not account for complex material properties like viscoelasticity. Future work could focus on integrating dynamic adaptation, leveraging machine learning to predict optimal resolutions, extending support for complex materials, and exploring hybrid methods that combine precomputation with dynamic refinement. Testing the framework in more diverse real-world scenarios, such as extreme motions, could further enhance its versatility and robustness.



Fig. 20. Wine Style Dress. Comparing our method to a full simulation with a uniform fine resolution and dynamic remeshing [Narain et al. 2012] during simulation runtime. Our method achieves results comparable to the full simulation. In contrast, dynamic remeshing introduces noticeable artifacts.

## Acknowledgments

We wish to thank anonymous reviewers for valuable comments and Tianqi Gao for encouragement and support. This work was supported by Key R&D Program of Hangzhou (No. 2024SDZ1A20).

## References

- Hillel Aharoni, Desislava V Todorova, Octavio Albarrán, Lucas Goehring, Randall D Kamien, and Eleni Katifori. 2017. The Smectic Order of Wrinkles. *Nature communications* 8, 1 (2017), 15809.
- David Baraff and Andrew Witkin. 1998. Large Steps in Cloth Simulation. In *Proceedings of the 25th Annual Conference on Computer Graphics and Interactive Techniques (SIGGRAPH '98)*. Association for Computing Machinery, New York, NY, USA, 43–54.
- Miklós Bergou, Saurabh Mathur, Max Wardetzky, and Eitan Grinspun. 2007. TRACKS: Toward Directable Thin Shells. *ACM Trans. Graph.* 26, 3 (jul 2007), 50–es.
- Sofien Bouaziz, Sébastien Martin, Tianjian Liu, Ladislav Kavan, and Mark Pauly. 2014. Projective Dynamics: Fusing Constraint Projections for Fast Simulation. *ACM Trans. Graph. (SIGGRAPH)* 33, 4, Article 154 (July 2014), 11 pages.
- Robert Bridson. 2007. Fast Poisson Disk Sampling in Arbitrary Dimensions. In *ACM SIGGRAPH 2007 Sketches* (San Diego, California) (SIGGRAPH '07). Association for Computing Machinery, New York, NY, USA, 22?es.
- Enrique Cerdá and Lakshminarayanan Mahadevan. 2003. Geometry and Physics of Wrinkling. *Physical review letters* 90, 7 (2003), 074302.
- Jiong Chen, Florian Schäfer, Jin Huang, and Mathieu Desbrun. 2021b. Multiscale Cholesky Preconditioning for Ill-Conditioned Problems. *ACM Trans. Graph.* 40, 4, Article 81 (jul 2021), 13 pages.
- Zhen Chen, Hsiao-Yu Chen, Danny M. Kaufman, Mélina Skouras, and Etienne Vouga. 2021a. Fine Wrinkling on Coarsely Meshed Thin Shells. *ACM Trans. Graph.* 40, 5, Article 190 (aug 2021), 32 pages.
- Zhen Chen, Danny Kaufman, Mélina Skouras, and Etienne Vouga. 2023. Complex Wrinkle Field Evolution. *ACM Trans. Graph.* 42, 4, Article 72 (jul 2023), 19 pages.
- Kwang-Jin Choi and Hyeong-Seok Ko. 2002. Stable but Responsive Cloth. *ACM Trans. Graph. (SIGGRAPH)* 21, 3 (July 2002), 604–611.
- Russell Gillette, Craig Peters, Nicholas Vining, Essex Edwards, and Alla Sheffer. 2015. Real-Time Dynamic Wrinkling of Coarse Animated Cloth. In *Proceedings of the 14th ACM SIGGRAPH / Eurographics Symposium on Computer Animation (Los Angeles, California) (SCA '15)*. Association for Computing Machinery, New York, NY, USA, 17–26.
- Sunil Hadap, E Bongarter, Pascal Volino, and Nadia Magnenat-Thalmann. 1999. Animating Wrinkles on Clothes. In *Proceedings Visualization '99 (Cat. No. 99CB37067)*. IEEE, 175–523.
- Timothy J Healey, Qingdu Li, and Ron-Bin Cheng. 2013. Wrinkling Behavior of Highly Stretched Rectangular Elastic Films via Parametric Global Bifurcation. *Journal of Nonlinear Science* 23 (2013), 777–805.

- Francois Labelle and Jonathan Richard Shewchuk. 2003. Anisotropic Voronoi Diagrams and Guaranteed-quality Anisotropic Mesh Generation. In *Proceedings of the nineteenth annual symposium on Computational geometry*. 191–200.
- Zorah Lahner, Daniel Cremers, and Tony Tung. 2018. Deepwrinkles: Accurate and Realistic Clothing Modeling. In *Proceedings of the European conference on computer vision (ECCV)*. 667–684.
- Lei Lan, Minchen Li, Chenfanfu Jiang, Huamin Wang, and Yin Yang. 2023. Second-Order Stencil Descent for Interior-Point Hyperelasticity. *ACM Trans. Graph.* 42, 4, Article 108 (jul 2023), 16 pages.
- Qiqin Le, Yitong Deng, Jiamu Bu, Bo Zhu, and Tao Du. 2023. Second-Order Finite Elements for Deformable Surfaces. In *SIGGRAPH Asia 2023 Conference Papers (SA '23)*. Association for Computing Machinery, New York, NY, USA, Article 113, 10 pages.
- Qingdu Li and Timothy J Healey. 2016. Stability Boundaries for Wrinkling in Highly Stretched Elastic Sheets. *Journal of the Mechanics and Physics of Solids* 97 (2016), 260–274.
- Hsueh-Ti Derek Liu, Mark Gillespie, Benjamin Chislett, Nicholas Sharp, Alec Jacobson, and Keenan Crane. 2023. Surface Simplification Using Intrinsic Error Metrics. *ACM Trans. Graph.* 42, 4, Article 118 (jul 2023), 17 pages.
- Miles Macklin, Matthias Müller, and Nuttapong Chentanez. 2016. XPBD: Position-Based Simulation of Compliant Constrained Dynamics. In *Proceedings of the 9th International Conference on Motion in Games* (Burlingame, California) (*MIG '16*). Association for Computing Machinery, New York, NY, USA, 49–54.
- Matthias Müller and Nuttapong Chentanez. 2010. Wrinkle Meshes. In *Proceedings of the 2010 ACM SIGGRAPH/Eurographics Symposium on Computer Animation* (Madrid, Spain) (*SCA '10*). Eurographics Association, Goslar, DEU, 85–92.
- Rahul Narain, Tobias Pfaff, and James F. O'Brien. 2013. Folding and Crumpling Adaptive Sheets. *ACM Trans. Graph. (SIGGRAPH)* 32, 4, Article 51 (July 2013), 8 pages.
- Rahul Narain, Armin Samii, and James F. O'Brien. 2012. Adaptive Anisotropic Remeshing for Cloth Simulation. *ACM Trans. Graph. (SIGGRAPH Asia)* 31, 6, Article 152 (Nov. 2012), 152:1–152:10 pages.
- Young Jin Oh, Tae Min Lee, and In-Kwon Lee. 2018. Hierarchical Cloth Simulation Using Deep Neural Networks. In *Proceedings of Computer Graphics International 2018* (Bintan, Island, Indonesia) (*CGI 2018*). Association for Computing Machinery, New York, NY, USA, 139–146.
- Joseph D Paulsen, Evan Hohlfeld, Hunter King, Jiangshui Huang, Zhanlong Qiu, Thomas P Russell, Narayanan Menon, Dominic Vella, and Benny Davidovitch. 2016. Curvature-induced Stiffness and the Spatial Variation of Wavelength in Wrinkled Sheets. *Proceedings of the National Academy of Sciences* 113, 5 (2016), 1144–1149.
- Tobias Pfaff, Meire Fortunato, Alvaro Sanchez-Gonzalez, and Peter Battaglia. 2020. Learning Mesh-Based Simulation with Graph Networks. In *International Conference on Learning Representations*.
- Tobias Pfaff, Rahul Narain, Juan Miguel de Joya, and James F. O'Brien. 2014. Adaptive Tearing and Cracking of Thin Sheets. *ACM Trans. Graph.* 33, 4, Article 110 (jul 2014), 9 pages.
- Tiberiu Popa, Quan Zhou, Derek Bradley, Vladislav Kraevoy, Hongbo Fu, Alla Sheffer, and Wolfgang Heidrich. 2009. Wrinkling Captured Garments using Space-time Data-driven Deformation. *Computer Graphics Forum* 28, 2 (2009), 427–435.
- Olivier Rémillard and Paul G. Kry. 2013. Embedded Thin Shells for Wrinkle Simulation. *ACM Trans. Graph.* 32, 4, Article 50 (jul 2013), 8 pages.
- Damien Rohmer, Tiberiu Popa, Marie-Paule Cani, Stefanie Hahmann, and Alla Sheffer. 2010. Animation Wrinkling: Augmenting Coarse Cloth Simulations with Realistic-Looking Wrinkles. *ACM Trans. Graph.* 29, 6, Article 157 (dec 2010), 8 pages.
- Nicholas Sharp, Yousuf Soliman, and Keenan Crane. 2019. Navigating Intrinsic Triangulations. *ACM Trans. Graph.* 38, 4, Article 55 (jul 2019), 16 pages.
- Jonathan Richard Shewchuk. 2002a. Delaunay Refinement Algorithms for Triangular Mesh Generation. *Computational geometry* 22, 1-3 (2002), 21–74.
- Jonathan Richard Shewchuk. 2002b. What is a Good Linear Element? Interpolation, Conditioning, and Quality Measures.. In *IMR*. 115–126.
- Oded Stein, Eitan Grinspun, and Keenan Crane. 2018. Developability of Triangle Meshes. *ACM Trans. Graph.* 37, 4, Article 77 (jul 2018), 14 pages.
- Rasmus Tamstorf, Toby Jones, and Stephen F. McCormick. 2015. Smoothed Aggregation Multigrid for Cloth Simulation. *ACM Trans. Graph. (SIGGRAPH Asia)* 34, 6, Article 245 (Oct. 2015), 13 pages.
- Hugues Vandeparre, Miguel Piñeirua, Fabian Brau, Benoit Roman, José Bico, Cyprien Gay, Wenzhong Bao, Chun Ning Lau, Pedro M Reis, and Pascal Damman. 2011. Wrinkling Hierarchy in Constrained Thin Sheets from Suspended Graphene to Curtains. *Physical Review Letters* 106, 22 (2011), 224301.
- Roman Vetter, Norbert Stoop, Falk K Wittel, and Hans J Herrmann. 2014. Simulating Thin Sheets: Buckling, Wrinkling, Folding and Growth. In *Journal of Physics: Conference Series*, Vol. 487. IOP Publishing, 012012.
- Huamin Wang. 2021. GPU-Based Simulation of Cloth Wrinkles at Submillimeter Levels. *ACM Trans. Graph.* 40, 4, Article 169 (jul 2021), 14 pages.
- Huamin Wang, Florian Hecht, Ravi Ramamoorthi, and James F. O'Brien. 2010. Example-Based Wrinkle Synthesis for Clothing Animation. *ACM Trans. Graph.* 29, 4, Article 107 (jul 2010), 8 pages.
- Huamin Wang and Yin Yang. 2016. Descent Methods for Elastic Body Simulation on the GPU. *ACM Trans. Graph. (SIGGRAPH Asia)* 35, 6, Article 212 (Nov. 2016), 10 pages.
- Ting Wang, Chenbo Fu, Fan Xu, Yongzhong Huo, and Michel Potier-Ferry. 2019. On the Wrinkling and Restabilization of Highly Stretched Sheets. *International Journal of Engineering Science* 136 (2019), 1–16.
- Zhendong Wang, Longhua Wu, Marco Fratarcangeli, Min Tang, and Huamin Wang. 2018. Parallel Multigrid for Nonlinear Cloth Simulation. *Computer Graphics Forum (Pacific Graphics)* 37, 7 (2018), 131–141.
- Zhendong Wang, Yin Yang, and Huamin Wang. 2023. Stable Discrete Bending by Analytic Eigensystem and Adaptive Orthotropic Geometric Stiffness. *ACM Trans. Graph.* 42, 6, Article 175 (Dec. 2023), 16 pages. doi:10.1145/3618372
- Martin Wicke, Daniel Ritchie, Bryan M. Klingner, Sebastian Burke, Jonathan R. Shewchuk, and James F. O'Brien. 2010. Dynamic Local Remeshing for Elastoplastic Simulation. *ACM Trans. Graph.* 29, Article 49 (July 2010), 11 pages. Issue 4.
- Botao Wu, Zhendong Wang, and Huamin Wang. 2022. A GPU-Based Multilevel Additive Schwarz Preconditioner for Cloth and Deformable Body Simulation. *ACM Trans. Graph.* 41, 4, Article 63 (jul 2022), 14 pages.
- Longhua Wu, Botao Wu, Yin Yang, and Huamin Wang. 2020. A Safe and Fast Repulsion Method for GPU-Based Cloth Self Collisions. 40, 1, Article 5 (dec 2020), 18 pages.
- Jiawang Yu and Zhendong Wang. 2024. Super-Resolution Cloth Animation with Spatial and Temporal Coherence. *ACM Trans. Graph.* 43, 4, Article 105 (July 2024), 14 pages. doi:10.1145/3658143
- Jiayi Eris Zhang, Jérémie Dumas, Yun (Raymond) Fei, Alec Jacobson, Doug L. James, and Danny M. Kaufman. 2022. Progressive Simulation for Cloth Quasistatics. *ACM Trans. Graph.* 41, 6, Article 218 (nov 2022), 16 pages.
- Evgeny Zuenko and Matthias Harders. 2019. Wrinkles, Folds, Creases, Buckles: Small-scale Surface Deformations as Periodic Functions on 3D Meshes. *IEEE Transactions on Visualization and Computer Graphics* 26, 10 (2019), 3077–3088.
- Javier S Zurdo, Juan P Brito, and Miguel A Otaduy. 2013. Animating Wrinkles by Example on Non-skinned Cloth. *IEEE Transactions on Visualization and Computer Graphics* 19, 1 (2013), 149–158.